

Progress in Clathrate Research

Silke Paschen, Michael Baenitz, Anders Bentien, Wilder Carrillo-Cabrera, F. Malte Grosche, Shin-ichi Kimura*, Vicente Pacheco, Ulrich Schwarz, Jörg Sichelschmidt, Paul Simon, Günter Sparn, Peter Thalmeier, Vladimir Voevodin, Alexander Yaresko, Huiqiu Yuan, Ivica Zerec, Yuri Grin and Frank Steglich

In this report we summarize the progress made since our last Scientific Report on clathrates [1] where we discussed the properties of $\text{Ba}_6\text{Ge}_{25}$ and $\text{Eu}_8\text{Ga}_{16}\text{Ge}_{30}$. Our main concern continues to be to discover new Kondo insulators in the family of clathrates or clathrate-like compounds. We have pursued this goal by different routes. An attempt was made to substitute Eu for Ba in $\text{Ba}_6\text{Ge}_{25}$ [2]. During this investigation a clathrate-like Eu phase, $\text{EuGa}_{2\pm x}\text{Ge}_{4\mp x}$ was found and characterized in detail [3]. In order to suppress the ferromagnetism and to promote a strongly correlated semiconducting (Kondo insulating) ground state in $\text{Eu}_8\text{Ga}_{16}\text{Ge}_{30}$ we have, on one hand, varied the stoichiometry around the ideal 8:16:30 composition [4-6] and, on the other hand, we have performed high-pressure studies [7,8]. However, the ferromagnetic transition temperature turned out to be very robust against both influences. Several attempts to synthesize new rare-earth containing clathrates were unsuccessful. The synthesis of such compounds might be favored by high pressures. Therefore, considerable effort has been put into building up a high-pressure synthesis facility (see chapter “*Synthesis at High Pressures and High Temperatures*” in this Report). Even though we have, up to now, not found any Kondo insulating clathrate, our research has led to other very interesting findings.

In $\text{Ba}_6\text{Ge}_{25}$, we have found a BCS-like superconducting transition at a resistive $T_c \approx 0.24$ K, which increases more than 16-fold as the “locking-in” phase transition is suppressed by hydrostatic pressure [9]. A detailed investigation of the superconducting state of $\text{Ba}_6\text{Ge}_{25}$ and the isostructural compound $\text{Ba}_4\text{Na}_2\text{Ge}_{25}$ [9-11], band structure calculations [12], and optical reflectivity experiments [13] have shed new light on the influence of the locking-in phase transition on the electronic structure of $\text{Ba}_6\text{Ge}_{25}$.

The stoichiometry-tuning experiments on $\text{Eu}_8\text{Ga}_{16}\text{Ge}_{30}$ have shown that the (few) charge carriers present in all samples are due to off-stoi-

chiometry and that $\text{Eu}_8\text{Ga}_{16}\text{Ge}_{30}$ samples with the ideal 8:16:30 composition would be insulators. Thus, we have shown the Zintl concept to be valid for $\text{Eu}_8\text{Ga}_{16}\text{Ge}_{30}$ [4,6]. Below we describe some of our results in more detail.

$\text{Ba}_{6-x}\text{M}_x\text{Ge}_{25}$ ($M = \text{Na}, \text{Eu}$)

Investigating the Ba-Eu-Ge system [2,3] we determined the solubility range of Eu in $\text{Ba}_6\text{Ge}_{25}$ [$a = 14.5565(2)$ Å]. For $\text{Ba}_{6-x}\text{Eu}_x\text{Ge}_{25}$ samples annealed at 630 °C the maximum substitution of Eu in the Ba sublattice is about 10 % ($x = 0.6$). In samples with $x > 0.6$, EuGe_2 and Ge appear as minority phases. The lattice parameter a varies linearly with the Eu content x at $x < 0.6$ but is constant at $x > 0.6$ (Fig. 1). Both $\text{Ba}_6\text{Ge}_{25}$ and $\text{Ba}_{5.4}\text{Eu}_{0.6}\text{Ge}_{25}$ melt incongruently (peritectically at about 816 °C and 806 °C, respectively). The sample $\text{Ba}_4\text{Na}_2\text{Ge}_{25}$ [$a = 14.4703(2)$ Å] was also prepared but the homogeneity range of $\text{Ba}_{6-x}\text{Na}_x\text{Ge}_{25}$ was not studied in detail [14]. Nevertheless, the study indicated that $x = 2$ represents the maximum Na solubility. An analysis of the crystal structure of $\text{Ba}_{5.4}\text{Eu}_{0.6}\text{Ge}_{25}$ [$a = 14.5271(2)$ Å] shows that the Eu atoms preferentially occupy the Ba1 and Ba3

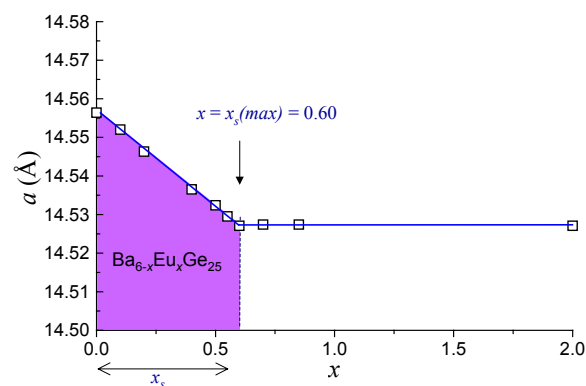


Fig. 1: Lattice parameter a vs. Eu content x of the target composition $\text{Ba}_{6-x}\text{Eu}_x\text{Ge}_{25}$.

sites (21 % and 34 %, respectively) and that in $\text{Ba}_4\text{Na}_2\text{Ge}_{25}$ the Na atoms occupy only the Ba2 site. A splitting of the Ba2 and Ba3 sites as observed in $\text{Ba}_6\text{Ge}_{25}$ [1,2] is also found for $\text{Ba}_{5.4}\text{Eu}_{0.6}\text{Ge}_{25}$ and $\text{Ba}_4\text{Na}_2\text{Ge}_{25}$ [14]. In order to test whether this splitting occurs randomly or in an ordered way we have investigated $\text{Ba}_6\text{Ge}_{25}$ by high-resolution transmission electron microscopy (HRTEM). As may be seen from Fig. 2 no superstructure reflections and no inhomogeneity in the HRTEM image are observed, pointing to a random splitting at least at room temperature.

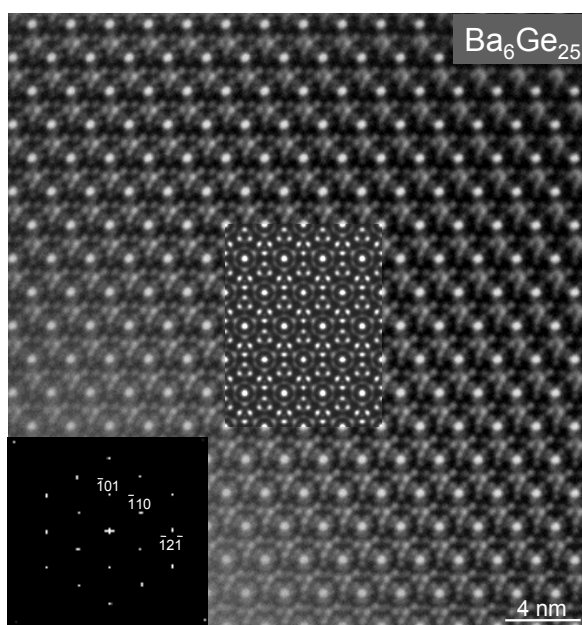


Fig. 2: HRTEM image (Philips CM200 FEG) of $\text{Ba}_6\text{Ge}_{25}$ at room temperature, [111] zone, with simulated image (inset middle) and corresponding processed Fast Fourier Transform (FFT) (inset, left bottom). The change in contrast at the right top is due to crystal thickness and bending. The FFT pattern does not show any superstructure reflections.

The two-step first-order locking-in phase transition, which occurs in $\text{Ba}_6\text{Ge}_{25}$ at $T_{S1,S2} \approx 215, 180$ K (average of warming and cooling curves), is quickly suppressed with increasing x in $\text{Ba}_{6-x}\text{Eu}_x\text{Ge}_{25}$ and is absent altogether in $\text{Ba}_4\text{Na}_2\text{Ge}_{25}$ [2,9]. The rate of decrease of $T_{S1,S2}$ with decreasing lattice parameter a is 5 times larger for $\text{Ba}_{6-x}\text{Eu}_x\text{Ge}_{25}$ upon increasing x than for $\text{Ba}_6\text{Ge}_{25}$ under (small) hydrostatic pressure [2,9]. Also, $\text{Ba}_4\text{Na}_2\text{Ge}_{25}$ should, according to its lattice parameter, undergo a structural transition at $T_S \approx 170$ K. Thus, the suppres-

sion of $T_{S1,S2}$ by alloying $\text{Ba}_6\text{Ge}_{25}$ with Eu or Na is stronger than a mere chemical pressure effect. According to magnetization and magnetic susceptibility measurements Eu is close to the f^7 state in $\text{Ba}_{6-x}\text{Eu}_x\text{Ge}_{25}$ [2]. It would be very interesting to obtain a *full* replacement of Ba at the Ba1 and Ba3 sites (or even at all three Ba sites) with Eu, i.e., $\text{Ba}_3\text{Eu}_3\text{Ge}_{25}$ (or $\text{Eu}_6\text{Ge}_{25}$) by the high-pressure synthesis to see whether Kondo lattice effects are observed. The fact that Ba locks into the split sites in $\text{Ba}_6\text{Ge}_{25}$ indicates that the guest/host interaction is stronger in $\text{Ba}_6\text{Ge}_{25}$ than in $\text{Eu}_8\text{Ga}_{16}\text{Ge}_{30}$, which does *not* behave as a Kondo lattice system.

Interplay of structural and superconducting transition in $\text{Ba}_6\text{Ge}_{25}$

The temperature dependence of the electrical resistivity $\rho(T)$ of $\text{Ba}_6\text{Ge}_{25}$ is presented in Fig. 3 for various pressures [9-11]. The main panel shows the high-temperature structural phase transition, the insets focus on the superconducting phase transition. The bulk nature of the superconductivity is inferred from measurements of the specific heat [9] and the magnetic susceptibility [11] in addition to this resistivity observation. At ambient pressure, $\rho(T)$ of $\text{Ba}_6\text{Ge}_{25}$ exhibits metallic behavior from room temperature down to about 230 K, followed at lower temperature by a two-step anomaly at $T_{S1,S2} \approx 230$ K, 196 K (on warming), which is due to the locking-in structural phase transition and which is accompanied by a steep increase of the resistivity to about $1 \text{ m}\Omega\text{cm}$. Below T_{S2} , the resis-

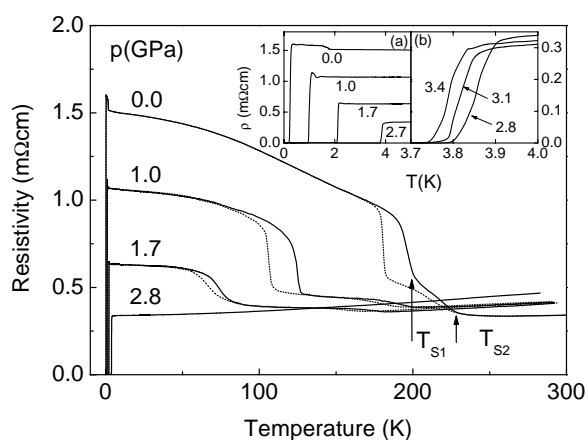


Fig. 3: Temperature dependence of the electrical resistivity $\rho(T)$ of $\text{Ba}_6\text{Ge}_{25}$ at different hydrostatic pressures p .

tivity continues to rise, saturating below 10 K at $\rho_0 \approx 1.5$ m Ω cm. At $T_x \approx 2$ K, there is another strongly sample-dependent resistive anomaly which might originate from sample inhomogeneities and grain boundaries [11]. Finally, a BCS-like superconducting transition with the mid-point of the resistivity jump at $T_c \approx 0.24$ K is observed [9,11]. With increasing pressure, the structural transitions are suppressed to lower temperatures and the residual resistivity ρ_0 is reduced. The low temperature anomaly disappears and T_c increases. At the critical pressure $p_c = 2.8$ GPa, where $T_{S1,S2}$ are completely suppressed, T_c reaches a maximum of about 3.8 K above which the resistivity is metallic with a poor residual resistance ratio. With further increasing pressure T_c decreases slightly. Interestingly, we found [11] that T_c decreases exponentially as a function of ρ_0 : $T_c \propto \exp(-\rho_0/\rho_c)$, where ρ_c is a constant.

The pressure dependence of the structural transition temperatures $T_{S1,S2}$ and the superconducting transition temperature T_c of $\text{Ba}_6\text{Ge}_{25}$ are summarized in a lattice parameter (pressure) - temperature phase diagram (Fig. 4). The lattice parameters are calculated by using the bulk modulus $B_0 = 44$ GPa and its pressure derivative $dB_0/dp = 5.8$ [15]. T_{S1} (the onset temperature) and T_{S2} (the mid-point of

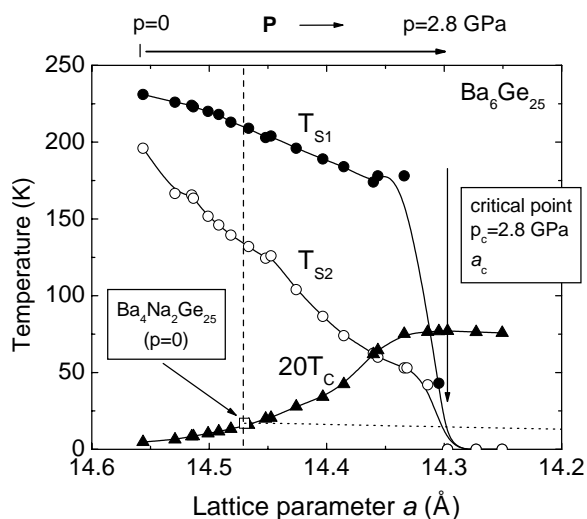


Fig. 4: Lattice parameter (pressure) - temperature phase diagram of $\text{Ba}_6\text{Ge}_{25}$. $T_{S1,S2}$ designate the structural transitions, T_c the superconducting transition. For comparison, the superconducting transition temperature ($20 T_c$) of $\text{Ba}_4\text{Na}_2\text{Ge}_{25}$ is shown as a dotted line. The lattice parameter of $\text{Na}_2\text{Ba}_4\text{Ge}_{25}$ at ambient pressure is denoted by a dashed line.

the sharp resistive jump) are determined from the warming-up data. T_{S1} and T_{S2} decrease linearly with increasing pressure below 2 GPa and are rapidly suppressed by pressure above 2 GPa. On the other hand, T_c undergoes a 16-fold increase from $T_c \approx 0.24$ K at $p = 0$ to $T_c \approx 3.85$ K at $p = p_c \approx 2.8$ GPa as the structural transition is suppressed. A comparison of the superconducting properties of $\text{Ba}_6\text{Ge}_{25}$ with those of the iso-structural compound $\text{Ba}_4\text{Na}_2\text{Ge}_{25}$ is most instructive. At ambient pressure, $\text{Ba}_4\text{Na}_2\text{Ge}_{25}$ lacks the structural transition and becomes superconducting at a higher T_c of approximately 0.84 K. According to low-temperature specific heat measurements [9], the density of states $N(E_F)$ inferred from the Sommerfeld coefficient is larger for $\text{Ba}_4\text{Na}_2\text{Ge}_{25}$ than for $\text{Ba}_6\text{Ge}_{25}$. Thus, the higher T_c of $\text{Ba}_4\text{Na}_2\text{Ge}_{25}$ at ambient pressure can qualitatively be understood with the simple BCS formula $T_c \propto \Theta_D \exp(-1/N(E_F)V)$, Θ_D and V being the Debye temperature and the pairing potential, respectively. As the structural distortion of $\text{Ba}_6\text{Ge}_{25}$ is suppressed by hydrostatic pressure, $\text{Ba}_6\text{Ge}_{25}$ and $\text{Ba}_4\text{Na}_2\text{Ge}_{25}$ behave similarly. However, $\text{Ba}_6\text{Ge}_{25}$ now shows a much higher T_c . These facts suggest that the structural transition may lead to a significant reduction of $N(E_F)$ and therefore to a very low T_c at ambient pressure [9,11]. To test this idea, we have performed an upper critical magnetic field study of the electrical resistivities of $\text{Ba}_6\text{Ge}_{25}$ and $\text{Ba}_4\text{Na}_2\text{Ge}_{25}$ under hydrostatic pressure [11]. We found that the initial slopes of the upper critical field, $(-dB_{c2}/dT)_{T_c}$, of both $\text{Ba}_6\text{Ge}_{25}$ and $\text{Ba}_4\text{Na}_2\text{Ge}_{25}$ are only weakly pressure dependent. In the ‘dirty’ limit, in which both samples were shown to be at all pressures [11], weak-coupling BCS theory gives $(-dB_{c2}/dT)_{T_c} = (4490 \text{ Tm}^2\text{K}^2/\Omega\text{J})\gamma\rho_0$ [16]. Since $\gamma \propto N(E_F)$, we can determine the pressure dependence of $N(E_F)$ from our experimental data of $(-dB_{c2}/dT)_{T_c}(p)$ and $\rho_0(p)$. The result is shown in Fig. 5 [11]. Indeed, $N(E_F)$ of $\text{Ba}_6\text{Ge}_{25}$ increases by a factor of 4 as the structural transition is suppressed, whereas $\text{Ba}_4\text{Na}_2\text{Ge}_{25}$ shows a weak decrease of $N(E_F)$ with increasing pressure. $N(E_F)$ of the undistorted form of $\text{Ba}_6\text{Ge}_{25}$ ($p \geq 2.8$ GPa) is larger than $N(E_F)$ of $\text{Ba}_4\text{Na}_2\text{Ge}_{25}$.

A detailed analysis [11] of the experimental data suggests that the pressure dependence of $N(E_F)$ dominates the pressure dependences of T_c in $\text{Ba}_6\text{Ge}_{25}$ for $p < p_c$. As stated above, T_c can be nicely fitted by $T_c \propto \exp(-\rho_0/\rho_c)$ as function of the residual resistivity ρ_0 . Comparing this with the BCS for-

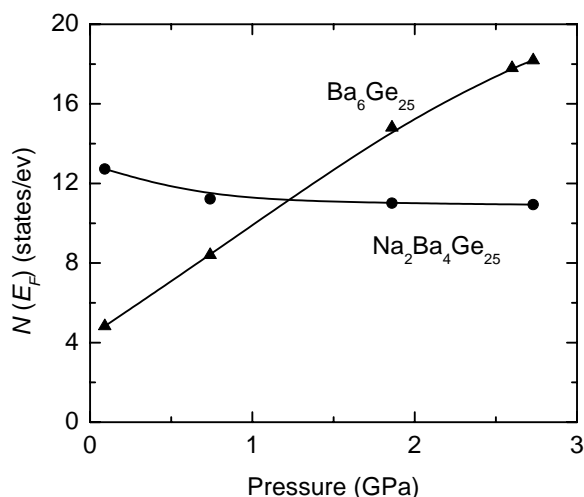


Fig. 5: Pressure dependence of the density of states per formula unit at the Fermi level $N(E_F)$ for Ba_6Ge_{25} and $Ba_4Na_2Ge_{25}$.

mula $T_c \propto \Theta_D \exp(-1/N(E_F)V)$ it follows that $\rho_0 \propto 1/N(E_F)(p)$ if the Debye temperature Θ_D and the pairing potential V are assumed to be pressure independent. In fact, the experimentally determined $\rho_0(p)$ plotted vs. $1/N(E_F)(p)$ (from Fig. 5) does follow this $\rho_0 \propto 1/N(E_F)(p)$ law. Also, $T_c(p)$ plotted vs. $1/N(E_F)(p)$ may be well described by $T_c = A \exp(-N/N(E_F))$, where A and N are constants. Thus, the pressure dependence of $N(E_F)$ alone can account for the strong enhancement of T_c as the structural distortion of Ba_6Ge_{25} is suppressed by pressure. Band structure calculations, to be presented below, show indeed the occurrence of a dip in the density of states at the Fermi level for distorted Ba_6Ge_{25} , which is absent for the undistorted form of Ba_6Ge_{25} .

Band structure of Ba_6Ge_{25} and $Ba_4Na_2Ge_{25}$

Our band structure calculations for the two clathrates, Ba_6Ge_{25} and $Ba_4Na_2Ge_{25}$, were performed within the local density approximation (LDA) using the LMTO method within the atomic sphere approximation. A scalar relativistic version was used with a von Barth-Hedin exchange-correlation potential [12].

The overall band structure (Fig. 6) is similar to the one of Ge in the diamond-type structure. In the bonding region, the band structure resembles the one of hypothetical empty Ge cages. However, the

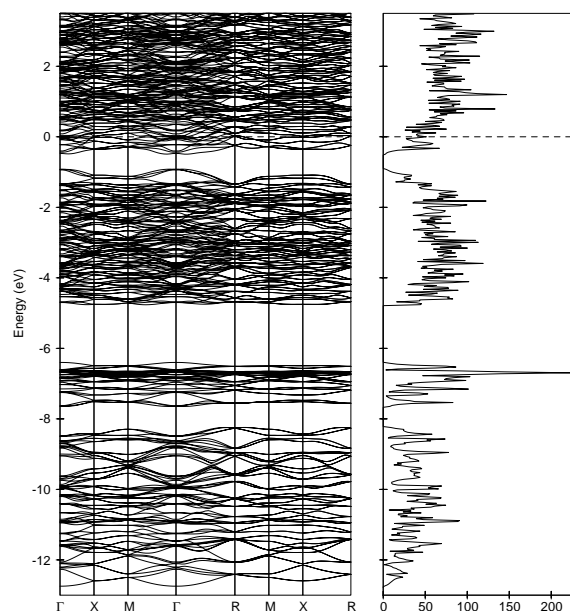


Fig. 6: Electronic band structure and density of states for Ba_6Ge_{25} in the low-temperature structure at 10 K with the Ba atoms in the average positions within the space group $P4_132$.

conduction bands, in particular at the Fermi level, have a strong contribution of Ba states. The analysis of the l -projected DOS shows that these states are of strong d -symmetry character. The calculations yield a peak of the DOS at the Fermi level that hints at the structural instabilities of the system.

It is assumed that, at the phase transition, the Ba2 atoms in Ba_6Ge_{25} are (randomly) locked to split sites [2, 17]. We have examined this effect by shifting the Ba2 atoms to one of the split sites. This leads to a splitting of the above described peak and a reduction of the DOS at the Fermi level (Fig. 7). This splitting, being due to the shifting of Ba2 atoms and the corresponding symmetry lowering, may be considered as a band Jahn-Teller effect. It should be noted that we did not take into account the effect of the random disorder of the locked-in Ba atoms.

In $Ba_4Na_2Ge_{25}$ there are also split sites, but there is no phase transition, i.e., no locking-in of either Ba or Na atoms, and it is plausible to perform the calculation keeping them at the average symmetric positions. Shifting Na or Ba atoms to one of the split positions does not produce a pronounced splitting of the peak in the DOS.

A locking-in of all Ba2 atoms in Ba_6Ge_{25} would result in a decrease of the value of the DOS by

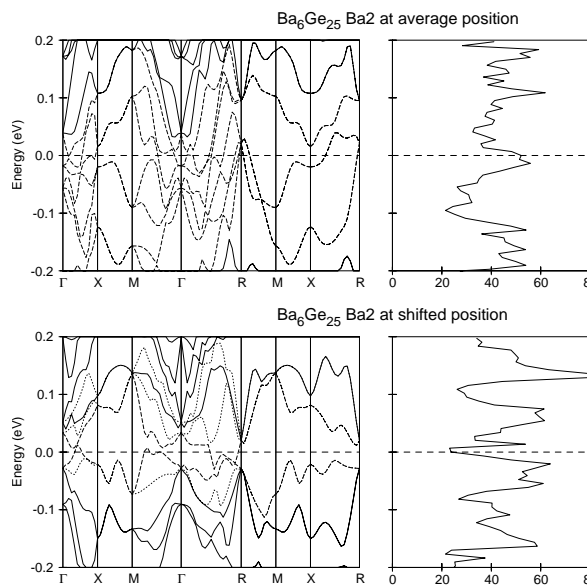


Fig. 7: Electronic band structure and density of states around the Fermi energy once for Ba2 at the average position and once for Ba2 shifted 80% toward the split site in $\text{Ba}_6\text{Ge}_{25}$. The dashed lines designate the bands that are crossing the Fermi level.

about 25 (eV)^{-1} per unit cell, which corresponds to a drop of the Pauli susceptibility by $2.08 \times 10^{-4} \text{ cm}^3/\text{mol}$ per formula unit, in order-of-magnitude agreement with the observed value. [2,17]. Moreover, the area of the Fermi surface is reduced because there are less bands crossing the Fermi level, as can be seen in Fig. 7. As a consequence, the electrical resistivity is expected to be enhanced below the locking-in phase transition, in agreement with the experimental observation.

The absolute value of the DOS at the Fermi level for distorted $\text{Ba}_6\text{Ge}_{25}$ (with Ba2 shifted) is 25 (eV)^{-1} (half of the value for undistorted $\text{Ba}_6\text{Ge}_{25}$). This corresponds to $\gamma = 15 \text{ mJ/molK}^2$ per formula unit. The experimental value is 21 mJ/molK^2 per formula unit [9]. For $\text{Ba}_4\text{Na}_2\text{Ge}_{25}$ we obtain 29 mJ/molK^2 per formula unit, where the experimental value is 33 mJ/molK^2 per formula unit. Introducing the calculated DOS values for distorted and undistorted $\text{Ba}_6\text{Ge}_{25}$ in the BCS formula $T_c \propto \Theta_D \exp(-1/N(E_F)V)$, a T_c ratio of 21 is obtained, in relatively good agreement with the observed ratio of 16. Thus, due to our band structure calculations, the DOS effect alone could account for the strong pressure variation of T_c in $\text{Ba}_6\text{Ge}_{25}$.

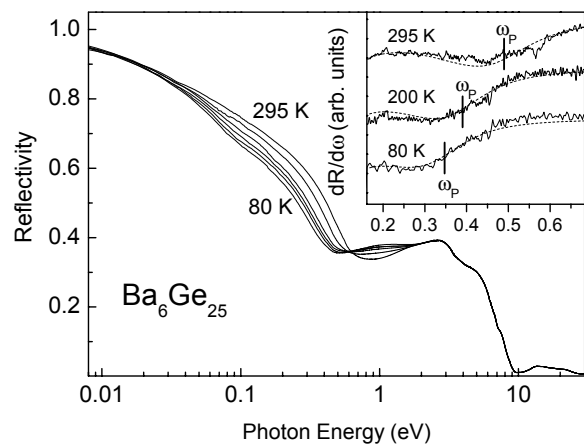


Fig. 8: Optical reflectivity R of $\text{Ba}_6\text{Ge}_{25}$ at several temperatures: From bottom to top, $T = 80, 140, 170, 200, 240, 295 \text{ K}$. Inset: First derivative of the reflectivity $dR/d\omega$. The dashed lines are Drude model fits as described in the text.

Optical reflectivity of $\text{Ba}_6\text{Ge}_{25}$

We have shown previously [2] that the Hall mobility μ_H of $\text{Ba}_6\text{Ge}_{25}$ decreases drastically as the system is cooled below the locking-in phase transition temperature. μ_H is determined by the effective mass m^* and the relaxation time τ via $\mu_H \propto \tau/m^*$. The reduction of μ_H may be due to a decrease of τ related to the enhanced disorder when Ba atoms lock *randomly* to split positions [9]. The results of our optical reflectivity measurements are shown in Fig. 8 [13]. A Drude-type electronic response, typical for systems with low charge-carrier concentration, dominates the reflectivity spectra at photon energies below 0.8 eV. We could fit the spectra with a Drude model with a temperature dependent plasma frequency $\omega_p(T)$ but a temperature *independent* relaxation time $\tau = (1.7 \pm 0.1) \times 10^{-14} \text{ s}$, as shown in the inset of Fig. 8. This would contradict our earlier assumption that the reduction of μ_H is due to a decrease of τ and would, instead, indicate that m^* increases. This interpretation is in agreement with the scenario of large bipolarons formed below the locking-in phase transition temperature proposed in Ref. 2. A low-temperature HRTEM investigation will be important to test whether the locking-in of the Ba atoms is really random.

Tuning the stoichiometry of $\text{Eu}_8\text{Ga}_{16}\text{Ge}_{30}$

The results described below will be published in a forthcoming paper [6]. Optical metallographic studies on a polished sample quenched from 1040 °C revealed that $\text{Eu}_8\text{Ga}_{16}\text{Ge}_{30}$ melts incongruently producing one majority and two minority phases.

The x-ray diffraction (XRD) pattern shows that the majority phase has the clathrate-I type structure [$a = 10.7059(1) \text{ \AA}$]. The weak intensity of the reflections of the minority phases makes their identification very difficult. The energy dispersive x-ray (EDX) analysis gave a Ga-poor composition for the clathrate-I phase, $\text{Eu}_{7.95(8)}\text{Ga}_{15.01(11)}\text{Ge}_{31.00(16)}$. The minority phases are a binary Ge-Ga eutecticum and a ternary Eu-Ga-Ge phase with compositions (in atomic %, standard deviations in parenthesis) 87(4):13(4) and 19.9(4): 71.5(5): 8.6(6), respectively. The latter one is $\text{EuGa}_{4-x}\text{Ge}_x$ with small x .

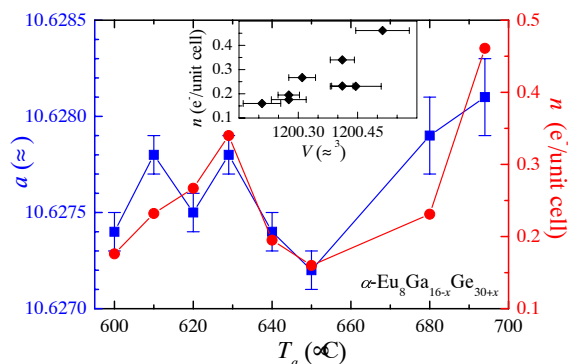


Fig. 9: Lattice parameter a and charge carrier concentration n vs. annealing temperature T_a for $\alpha\text{-Eu}_8\text{Ga}_{16-x}\text{Ge}_{30+x}$. The inset shows the variation of n with the volume V of the unit cell.

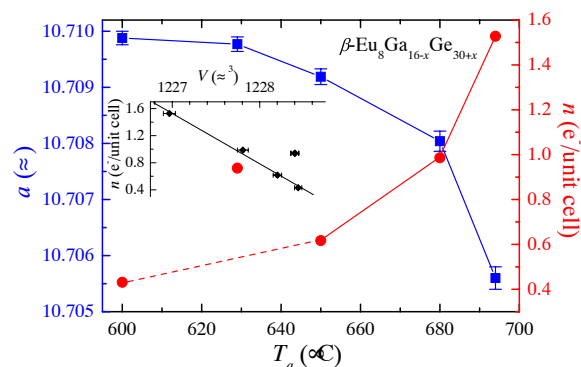


Fig. 10: Lattice parameter a and charge carrier concentration n vs. annealing temperature T_a for $\beta\text{-Eu}_8\text{Ga}_{16-x}\text{Ge}_{30+x}$. The inset shows the variation of n with the volume of the unit cell V .

The XRD patterns show that $\text{Eu}_8\text{Ga}_{16}\text{Ge}_{30}$ crystallizes in one of the two possible structure types, clathrate-I or -VIII type, depending on the thermal treatment. Samples quenched from high temperature (1040 °C) and then annealed present the $\alpha\text{-Eu}_8\text{Ga}_{16}\text{Ge}_{30}$ structure (space group $I4\bar{1}m$, clathrate-VIII type structure) while slow cooling of melted samples up to the annealing temperature produces $\beta\text{-Eu}_8\text{Ga}_{16}\text{Ge}_{30}$ (space group $Pm\bar{3}n$, clathrate-I type structure). It was found that the lattice parameters a of α - (Fig. 9) and of β - $\text{Eu}_8\text{Ga}_{16}\text{Ge}_{30}$ (Fig. 10) correlate with the annealing temperature T_a . The variations are larger in the β modification than in the α form: The maximal differences are 0.0043 Å and 0.0009 Å, respectively. In spite of the rather large scattering of the $a(T_a)$ data for the α samples, one can identify a trend to have smaller a at $T_a < 687 \text{ °C}$ [$a = 10.6281(2) \text{ \AA}$]. The smallest value of $a = 10.6272(1) \text{ \AA}$ is found at $T_a = 650 \text{ °C}$. $a(T_a)$ of the β samples shows a monotonic behavior. In contrast to the α samples, the smallest value of $a = 10.7056(2) \text{ \AA}$ is observed at the highest $T_a = 697 \text{ °C}$ for the β samples. With decreasing T_a , a increases and tends to a constant value of $a \approx 10.7099(1) \text{ \AA}$ at $T_a \leq 600 \text{ °C}$. We assumed that different annealing temperatures cause different changes of the Ga/Ge ratio inside the narrow homogeneity range of $\text{Eu}_8\text{Ga}_{16-x}\text{Ge}_{30+x}$. The EDX analysis of 4 selected samples gives 8 Eu guest atoms and 46 Ga/Ge framework atoms per formula unit, as expected. However, a significant deviation from the starting $\text{Ga}_{16}\text{Ge}_{30}$ ratio is found, namely $\text{Eu}_8\text{Ga}_{15.7}\text{Ge}_{30.3}$ and $\text{Eu}_8\text{Ga}_{15.3}\text{Ge}_{30.7}$ for the α and β phase, respectively. Thus, the β phase is more Ga deficient than the α phase. The small differences in the Ga content among samples of the same structure type are difficult to detect. Nevertheless, the above discussed variation of a indicates that a small homogeneity range between the Ga and Ge framework atoms does exist. An increase of a with Ga content was observed for $\text{Sr}_8\text{Ga}_{16-x}\text{Ge}_{30+x}$ [18] and for $\text{Ba}_8\text{Ga}_8\text{Si}_{36}$ [$a = 10.4350(1) \text{ \AA}$] and $\text{Ba}_8\text{Ga}_{12}\text{Si}_{33}$ [$a = 10.4705(2) \text{ \AA}$] [19].

We have performed Hall effect measurements on both α - and β - $\text{Eu}_8\text{Ga}_{16}\text{Ge}_{30}$. The charge carrier concentration n was obtained from the Hall coefficient data at 2 K by correcting the data for the anomalous Hall effect and by using a one band model. It is surprising how well n tracks the $a(T_a)$ dependence for the α samples (Fig. 9). For the β

samples, on the other hand, n increases with T_a in contrast to a , which decreases with T_a (Fig. 10) [4]. With the exception of a few outlying points, a linear relationship between n and the unit cell volume V is observed for both α - and β - $\text{Eu}_8\text{Ga}_{16-x}\text{Ge}_{30+x}$ (insets of Figs. 9 and 10). In the Zintl picture, the number of electrons per formula unit (or per unit cell) in $\text{Eu}_8\text{Ga}_{16-x}\text{Ge}_{30+x}$ would correspond to the value of x . According to our EDX results, $0.3 < x < 0.6$, in plausible agreement with the measured charge carrier concentration $0.15 < n < 1.5$ in electrons per unit cell. We conclude that the charge carriers observed in α - and β - $\text{Eu}_8\text{Ga}_{16-x}\text{Ge}_{30+x}$ are due to small deviations from the ideal $\text{Ga}_{16}:\text{Ge}_{30}$ stoichiometry.

Improved thermoelectric properties of stoichiometry-tuned $\text{Eu}_8\text{Ga}_{16-x}\text{Ge}_{30+x}$

In order to investigate the influence of the off-stoichiometry on the thermoelectric properties of α - and β - $\text{Eu}_8\text{Ga}_{16-x}\text{Ge}_{30+x}$, we have measured the temperature dependences of the electrical resistivity $\rho(T)$, the thermopower $S(T)$, and the thermal conductivity $\kappa(T)$ of all samples exploited in Figs. 9 and 10. A detailed description of this work will be published in a forthcoming paper [5]. Our earlier results [1,20] were obtained on the α and the β sample with the highest T_a of 694 °C. $\rho(T)$, $S(T)$, and $\kappa(T)$ of the new samples annealed at $T_a < 690$ °C are in overall agreement with these earlier results. However, details of these properties vary systematically with the charge carrier concentration n , as we shall show below.

For all samples, ρ increases with T (positive $d\rho/dT$), except for a narrow range above the ferromagnetic ordering temperature where $(d\rho/dT)$ is negative. For both the α and the β sample series, this anomalous behavior becomes more pronounced with decreasing n . We have earlier associated the negative $(d\rho/dT)$ with the scattering of the charge carriers from critical magnetic fluctuations [20]. A better screening of these fluctuations in samples with higher n is a plausible explanation for the above observation. The variation with n of the residual resistance ratio $\text{RRR} = \rho(400 \text{ K})/\rho(2 \text{ K})$ and of the residual resistivity ρ_0 taken as ρ at 2 K is shown in Fig. 11. There is a clear tendency that, for decreasing n , RRR decreases and ρ_0 increases, i.e., the samples become less metallic.

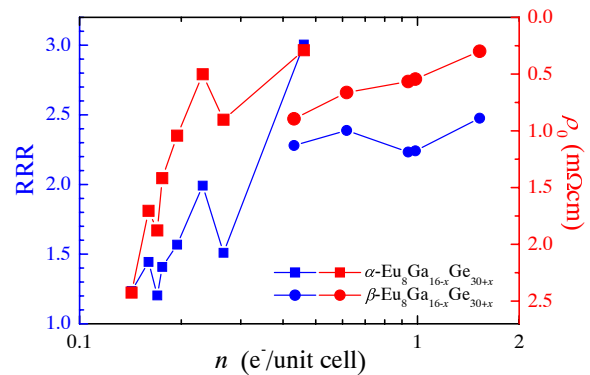


Fig. 11: Residual resistance ratio $\text{RRR} = \rho(400 \text{ K})/\rho(2 \text{ K})$ and residual resistivity $\rho_0 = \rho(2 \text{ K})$ (with inverted y axis) vs. charge carrier concentration n for α - and β - $\text{Eu}_8\text{Ga}_{16-x}\text{Ge}_{30+x}$.

With increasing T , the absolute value of the thermopower $|S|$ increases for all samples. S is negative in agreement with the charge carriers being electron-like. In Fig. 12 we show that the room temperature value of $|S|$ increases with decreasing n , as expected for a diffusion thermopower. At $n \approx 0.45$ electrons per unit cell, $|S|$ of β - $\text{Eu}_8\text{Ga}_{16-x}\text{Ge}_{30+x}$ is almost twice as large as $|S|$ of α - $\text{Eu}_8\text{Ga}_{16-x}\text{Ge}_{30+x}$. This may indicate that the effective mass of the charge carriers is larger for β - than for α - $\text{Eu}_8\text{Ga}_{16-x}\text{Ge}_{30+x}$.

The temperature dependence of κ is quite different for the α and the β samples. For the α samples the electronic contribution κ_e , calculated from the electrical resistivity using the Wiedemann-Franz law, is less than 1 % of κ at $T < 10 \text{ K}$ and about 30 % of κ at room temperature. For the β samples, κ_e

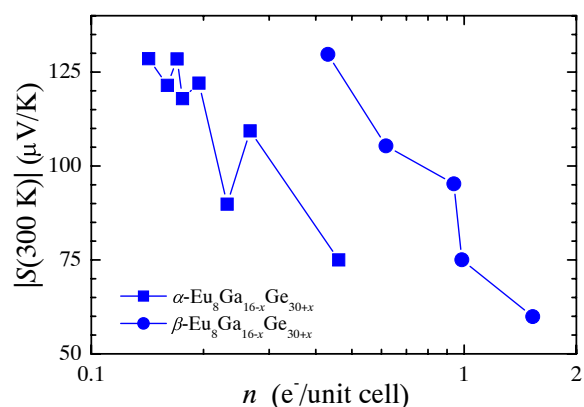


Fig. 12: Absolute value of the thermopower $|S|$ at 300 K vs. charge carrier concentration n for α - and β - $\text{Eu}_8\text{Ga}_{16-x}\text{Ge}_{30+x}$.

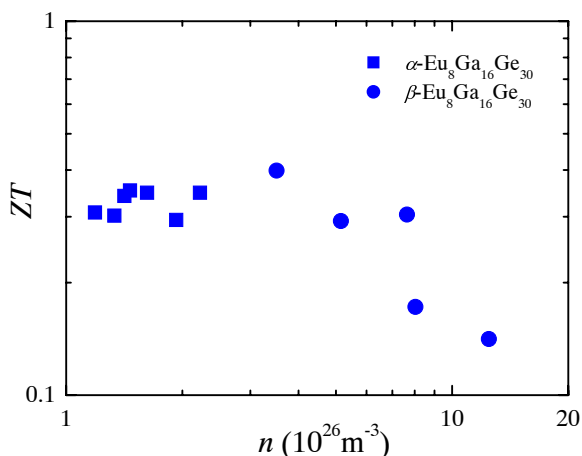


Fig. 13: Dimensionless thermoelectric figure of merit ZT at 400 K vs charge carrier concentration n for α - and β - $\text{Eu}_8\text{Ga}_{16-x}\text{Ge}_{30+x}$

is less than 15 % of κ below 10 K and about 50 % of κ at room temperature. The lattice contribution κ_1 of the α - $\text{Eu}_8\text{Ga}_{16-x}\text{Ge}_{30+x}$ samples has a temperature dependence similar to the one observed for crystalline materials. However, below approximately 4 K, the expected T^3 dependence is not observed. Instead, κ_1 of the α samples shows a T^ϵ dependence with ϵ being 1.1 to 1.5, typical of structural glasses and clearly observed at low temperatures for $\text{Sr}_8\text{Ga}_{16}\text{Ge}_{30}$ [21] and $\text{Ba}_8\text{Ga}_{16}\text{Ge}_{30}$ [4]. $\kappa_1(T)$ of the β samples is glass-like in the entire temperature range, in qualitative agreement with earlier published data [22].

The dimensionless thermoelectric figure of merit $ZT = S^2/\rho\kappa$ calculated from the $\rho(T)$, $S(T)$, and $\kappa(T)$ data discussed above is shown in Fig. 13 for $T = 400$ K. For the β samples, ZT increases steeply with decreasing n , reaching $ZT \approx 0.4$ at $n = 3.5 \times 10^{26} \text{ m}^{-3}$. This is the highest ZT value ever found for a clathrate. Further experiments will have to show whether the trend of increasing ZT with decreasing n continues for even lower n , which might result in $ZT \geq 1$ attractive for thermoelectric applications. For the α samples, on the other hand, ZT is almost independent of n and ranges between 0.29 and 0.35 for the samples investigated here. A discussion of possible reasons for the different thermoelectric properties of α - and β - $\text{Eu}_8\text{Ga}_{16-x}\text{Ge}_{30+x}$ will be made in Ref. 5.

Can the ferromagnetic order be suppressed in $\text{Eu}_8\text{Ga}_{16}\text{Ge}_{30}$?

We have measured [5] the temperature dependence of the magnetic susceptibility $\chi(T)$ and the magnetic field dependence of the magnetization $M(H)$ of all samples of Figs. 9 and 10. $\chi(T)$ is Curie-Weiss-like above approximately 100 K, with effective moments which are in good agreement with the moment of free Eu^{2+} for all samples. Also, the saturation magnetization M_s at 2 K agrees approximately with the one expected for free Eu^{2+} moments. Thus, we have no indication for a moment reduction due to the Kondo effect. The Curie temperature T_C is almost the same for all the α - (or β -) $\text{Eu}_8\text{Ga}_{16}\text{Ge}_{30}$ samples. This is rather surprising since we believe the ferromagnetism in $\text{Eu}_8\text{Ga}_{16}\text{Ge}_{30}$ to be due to the RKKY interaction, where a dependence of T_C on the charge carrier concentration n may be expected [20]. T_C is also very robust against the application of hydrostatic pressure. It increases only slightly with pressure up to $p = 2.5$ GPa [7]. This is in accord with the smooth variation of the unit cell volume with pressure as determined from x-ray diffraction patterns of α - and β - $\text{Eu}_8\text{Ga}_{16}\text{Ge}_{30}$ (Fig. 14) [8]. Thus, the ferromagnetism in $\text{Eu}_8\text{Ga}_{16}\text{Ge}_{30}$ cannot be appreciably influenced by the variations of n and p studied so far.

Fig. 14: Unit cell volume vs. pressure for α - and β - $\text{Eu}_8\text{Ga}_{16}\text{Ge}_{30}$. Experimental data are indicated by symbols. The lines represent results of least-squares fits of Murnaghan-type equations to the experimental data, with V_0 fixed to the experimentally observed volume at ambient conditions. For α - $\text{Eu}_8\text{Ga}_{16}\text{Ge}_{30}$, data up to a maximum pressure of 8 GPa were taken into account for the fitting procedure. The experimental x-ray diffraction patterns were collected using synchrotron radiation at the ESRF, Grenoble.

References

- [1] *S. Paschen, W. Carrillo-Cabrera, M. Baenitz, V. H. Tran, A. Bentien, H. Borrmann, R. Cardoso Gil, R. Michalak, Yu. Grin, and F. Steglich*, in *Development of the Institute and Scientific Report* (Max-Planck-Institut für Chemische Physik fester Stoffe, Dresden, Germany, Nov. 2000).
- [2] *S. Paschen, V. H. Tran, M. Baenitz, W. Carrillo-Cabrera, Yu. Grin, and F. Steglich*, *Phys. Rev. B* **65**, 134435 (2002).
- [3] *W. Carrillo-Cabrera, S. Paschen, and Yu. Grin*, *J. Alloys Comp.* **333**, 4 (2002).
- [4] *S. Paschen, V. Pacheco, A. Bentien, A. Sanchez, W. Carrillo-Cabrera, M. Baenitz, B. B. Iversen, Yu. Grin, and F. Steglich*, to appear in *Physica B* (Proc. T²PAM).
- [5] *A. Bentien et al.*, to be submitted to PRB.
- [6] *V. Pacheco et al.*, to be submitted to PRB.
- [7] *H. Q. Yuan, et al.*, unpublished.
- [8] *U. Schwarz et al.*, unpublished.
- [9] *F. M. Grosche, H. Q. Yuan, W. Carrillo-Cabrera, S. Paschen, C. Langhammer, F. Kromer, G. Sparn, M. Baenitz, Yu. Grin, and F. Steglich*, *Phys. Rev. Lett.* **87**, 247003 (2001).
- [10] *H. Q. Yuan, F. M. Grosche, W. Carrillo-Cabrera, S. Paschen, G. Sparn, M. Baenitz, Yu. Grin, and F. Steglich*, *High Pressure Research* **22**, 147 (2002).
- [11] *H. Q. Yuan*, PhD thesis, TU Dresden, Germany, 2003 (unpublished).
- [12] *I. Zerec, A. Yaresko, P. Thalmeier, and Yu. Grin*, *Phys. Rev. B* **66**, 045115 (2002).
- [13] *J. Sichelschmidt, V. Voevodin, S. Paschen, W. Carrillo-Cabrera, Yu. Grin, and F. Steglich*, to appear in *Acta Physica Polonica* (Proc. SCES02).
- [14] *W. Carrillo-Cabrera, J. Curda, K. Peters, S. Paschen, Yu. Grin, and H.G. von Schnering*, *Z. Kristallogr. NCS* **216**, 183 (2001).
- [15] *V. Pacheco et al.*, unpublished.
- [16] *T. P. Orlando, E. J. McNiff, Jr., S. Foner, and M. R. Beasley*, *Phys. Rev. B* **19**, 4545 (1979).
- [17] *S. Paschen, V. H. Tran, M. Baenitz, W. Carrillo-Cabrera, R. Michalak, Yu. Grin, and F. Steglich*, in *Proceedings of the 19th International Conference on Thermoelectrics*, edited by D. M. Rowe (Babrow Press Wales, UK, 2000), p. 374.
- [18] *W. Carrillo-Cabrera, R. Cardoso Gil, and Yu. Grin*, *Z. Kristallogr. NCS* **217**, 179 (2002).
- [19] *Ya. Mudryk, P. Rogl, C. Paul, S. Berger, E. Bauer, G. Hilscher, C. Godart, and H. Noël*, *J. Phys.: Condens. Matter* **14**, 7991 (2002).
- [20] *S. Paschen, W. Carrillo-Cabrera, A. Bentien, V. H. Tran, M. Baenitz, Yu. Grin, and F. Steglich*, *Phys. Rev. B* **64**, 214404 (2001).
- [21] *J. L. Cohn, G. S. Nolas, V. Fessatidis, T. H. Metcalf, and G. A. Slack*, *Phys. Rev. Lett.* **82**, 779 (1999).
- [22] *G. S. Nolas, T. J. R. Weakley, J. L. Cohn, and R. Sharma*, *Phys. Rev. B* **61**, 3845 (2000).

* UVSOR Facility, Institute of Molecular Science, Okazaki 444-8585, Japan.